Intelligent supramolecular assembly of aromatic block molecules in aqueous solution

Wen Li,* Yongju Kim and Myongsoo Lee*

The construction of supramolecular nanoscopic architectures has been intensively pursued because of their unique features for applications in nanoscience and biomimetic chemistry. Molecular self-assemblies of aromatic rod–coil amphiphiles consisting of rigid rod segments and hydrophilic flexible chains in aqueous solution provide a facile avenue into this area. This feature article highlights the recent progress regarding the construction of aqueous assemblies that result from the sophisticated design of aromatic rod–coils, with the aim to develop stimuli-responsive systems and bioactive materials. Important factors affecting the self-assembly morphologies are discussed and summarized. Dynamic structural changes triggered by temperature and guest molecules are demonstrated. Finally, the perspective of bioactive nanostructures originated from self-assembly of aromatic block amphiphiles is also introduced.

1 Introduction

Supramolecular nanostructures produced *via* self-assembling molecules have attracted immense interest because the sophisticated structures formed through weak noncovalent interactions can be triggered by external stimuli leading to dynamic materials and nano-sensors.[1–3] Typical examples of basic building blocks for self-assembly include lipid molecules,[4] surfactants,[5] supra-amphiphiles,[6] block molecules,[7] hyper-branched polymers,[8] peptide derivatives[9] and inorganic/organic complexes.[10] Among them, rigid-flexible block molecules, consisting of aromatic rod and coil segments, are promising candidates for fabricating self-assembled structures.[11] Depending on their molecular topology and shapes, the rigid–flexible molecules can self-assemble into diverse liquid crystal structures, such as smectic, columnar, cubic and polygonal cylinder phases.[12–16] Besides the bulk nanostructures, the amphiphilic combination of the aromatic rod segments and the hydrophilic coil opens up a new possibility to exploit very interesting assemblies in aqueous solution.[17–20]

Aqueous assemblies have great advantages for the creation of desired materials in terms of biological applications, including tissue regeneration, drug delivery and ion channel regulation.[21–23] For the aqueous self-assembly of amphiphilic rigid-flexible block molecules, the hydrophobic rod and the hydrophilic coil have a strong tendency to segregate into their distinct own subspace due to structural flexibility contrast between the dissimilar segments. The energetic penalties associated with chain stretching of the coil block and interfacial energy drive the rod–coil blocks to self-assemble into well-ordered arrangements even the molecular weights of each block are very low. In addition, the anisotropic orientation of the stiff rod-like segments and the microsegregation of the incompatible molecular parts are able to enhance each other in water leading to the formation of thermodynamically stable supramolecular structures with a rigid hydrophobic core surrounded by flexible hydrophilic chains.[24–27] In general, monodisperse rod–coil blocks display highly reproducible and predictable self-assembly behavior.

Recently, pioneering studies have been performed on the development of diverse aqueous assemblies, such as tubules, toroids, porous capsules, and helical fibers, by adjusting the relative volume fraction between hydrophobic and hydrophilic segments of rod–coil molecules consisting of aromatic units and poly(propylene oxide) (PPO) or poly(ethylene oxide) (PEO) coils.[28–33] Emphasis has been placed on two characteristic features in these aqueous self-assembling nanostructures. One feature is the well-known lower critical solution temperature (LCST) property of the ethylene oxide segments, exhibiting a reversible hydration–dehydration transition in response to temperature.[34] The other is the arrangement and orientation of the rigid aromatic rod units, which have a propensity to transform rapidly into their equilibrium states when faced with very small variations in local environment. Small environmental changes are expected to affect significantly the packing model of aromatic rods and thus the ultimate structures of supramolecular assemblies. The combination of these two features in single molecules allows the self-assembled nanostructures to respond to different stimuli, such as certain guests, pH, solvent, temperature, light,[35] magnetic field[36] and redox,[18] by changing

State Key Lab of Supramolecular Structure and Materials, Jilin University, Changchun, 130012, China. E-mail: wenli@jlu.edu.cn; mslee@jlu.edu.cn; Fax: +86 431-85193421; Tel: +86 431-85168499

their shape or macroscopic properties. Normally, this change is fully reversible once the stimulus has been removed.

In this article, we focus on the recent progress in the development of aqueous nanostructure from the self-assembly of rod–coil block molecules. Here, we classified rod–coil molecules into two types. The first part covers the most widely studied rod–coils, in which the rod units are based on rigid aromatic scaffolds. We show the influence of volume fraction, molecular shape and the topology of rod units on the self-assembly behavior of aromatic block molecules. We also demonstrate how the self-assemblies exhibit adaptive properties to the temperature with the aim of the construction of smart materials. The second part is focused on the self-assembly of bioactive rod–coil molecules such as β-sheet peptide-based blocks and carbohydrate-based rod–coils. We highlight some possible applications in the field of biosciences.

2   Aqueous assembly from terminally grafted rod–coil amphiphiles

Rod–coil molecules consisting of rigid aromatic rods as a hydrophobic part and flexible poly(ethylene oxide) (PEO) chains as a hydrophilic part exhibit typical amphiphilic characteristics. The self-assembly of the rod–coil amphiphiles is dependent on the volume ratio of two dissimilar blocks. Jiang and co-workers[37] reported the self-assembly behavior of a tetrathiophene connecting triethylene oxide diblock molecule **1** (Fig. 1), which forms vesicular structures with a diameter of 80 nm. Cryo-TEM images show that the uni-lamellar vesicles have an elliptical shape. This shape is proposed by anisotropic packing of the tetrathiophene units to maximize the rod-to-rod interactions. In contrast, the molecule **2** based on a phenylene vinylene rod and a poly(ethylene) oxide coil self-assembles into long cylindrical micelles.[38] The diameter of the long fibers can be manipulated by controlling the repeating unit of the aromatic rod which comprises the inner core. The authors suggest that the arrangement of the rod units inside the micelles seems to adopt monolayer packing with interdigitated rod domains. In comparison with **1**, the longer rod segment of **2** provides stronger hydrophobic and π–π interactions, which suppress the high interface curvature and result in the formation of 1D nanofibers of several thousand nanometers in length. Following the above results, it is envisioned that coil–rod–coil molecules carrying hydrophilic PEO chains and oligo-*p*-phenylene as an elongated rod should show similar behavior as that of rod–coil building blocks. The coil–rod–coil molecule (**3**) self-assembles into micellar aggregates with a hydrophobic core, which provides a supramolecular reactor for aromatic coupling reactions in aqueous media. The coupling reactions of bromobenzenes or aryl chloride take place with quantitative conversion.

Aromatic rods connecting hydrophilic dendrons to both terminals can be considered as a new kind of amphiphilic block molecule because the tree-shaped molecule consists of hydrophilic dendritic chains as the head and a hydrophobic rod as the stem.[29] The dumbbell-shaped amphiphile has been synthesized through the connection between a conjugated rod
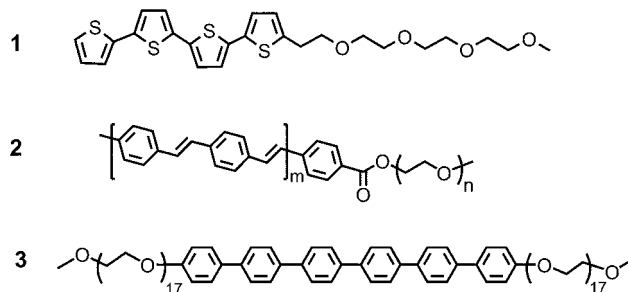

Fig. 1 Schematic structures of block molecules **1–3**.

and hydrophilic dendrons, which gives rise to the formation of helical nanostructures.[31] In a subsequent work, Lee and co-workers tried to explore the responsive characteristics of the self-assembled nanofibers such as their structural changes or related physical property changes upon the addition of guest molecules. For this purpose, they synthesized the dumbbell-shaped block molecule **4** consisting of hexa(*para*-phenylene) rod segment and EO dendritic chains with chiral carbon centers and investigated its self-assembly behavior in aqueous solution (Fig. 2).[39] When molecular dumbbell **4** was dissolved in water, the steric repulsion between bulky dendritic coils restrains the parallel arrangement of the hydrophobic rod segments. Thus, the rod segments stacked on top of each other with mutual rotation in the same direction to minimize the steric hindrance through microphase separation and hydrophobic interactions, leading to the formation of helical objects (Fig. 2). The one-handed helical sense is induced by transfer of chiral information from the molecular to supramolecular level. Interestingly,
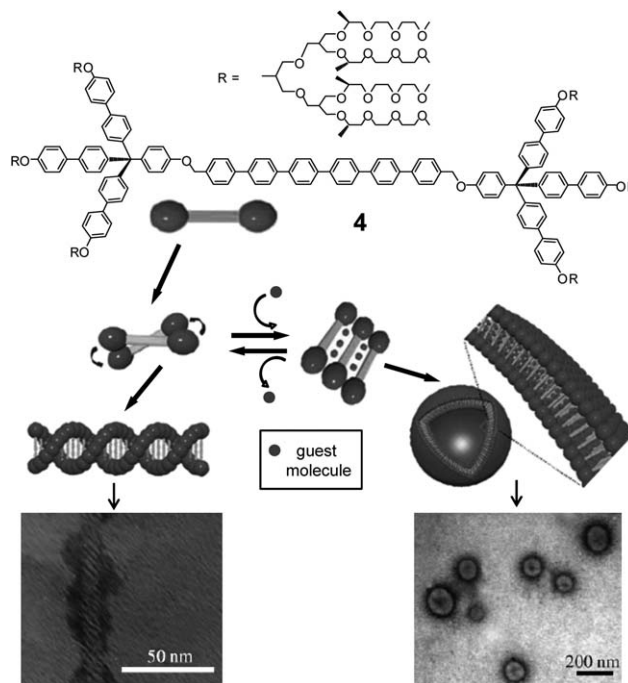

Fig. 2 Molecular structure of dumbbell-shaped amphiphile **4**, and schematic representation of structural interconversion between helical fibers and nanocapsules. Reproduced with permission from ref. 39. Copyright 2006 Wiley-VCH.

these obtained helices transform into nanocages with the addition of aromatic guest molecules such as 4-bromonitrobenzene (Fig. 2). In aqueous solution, aromatic guest molecules should locate at the hydrophobic core of the helical fibers *via* intermolecular interactions, leading to an enlarged distance between the adjacent rod segments. Subsequently, the twisted packing of the rod units is rearranged into parallel stacking. The parallel arrangement of the rod segments eventually leads to the formation of hollow capsules. After removing the guest molecule through extraction by organic solvent, the hollow capsules reconvert into helical nanofibers.

Molecular dumbbell **5**, consisting of a carbazole end-capped hexa-*p*-phenylene as an aromatic rod and chiral oligo(ethylene oxide) dendrons, self-assembles into nonchiral fibers in methanol solution (Fig. 3). These nanofibers were shown to recognize solvent polarity changes by inducing supramolecular chirality.[40] The TEM image of an aqueous solution of **5** revealed 1D elongated fibers with a uniform diameter of 4.8 nm. The CD spectra of **5** at room temperature displayed silent signals even though **5** contains chiral side groups, indicating that the fibrillar objects are nonchiral. Notably, the CD spectra showed a strong Cotton effect as the 60% water addition, indicative of the transformation of the fibers with supramolecular chirality. This chirality switching of the fibers is attributed to the conformational change of aromatic rod units and variation in hydrodynamic volumes. As confirmed by UV/vis and fluorescence measurements, the addition of water into methanol solution strengthened the hydrophobic and π–π interactions due to the increased polarity, which drives the rod segments to become more planar for closer packing to result in steric constraints, giving rise to a helical arrangement. Besides the 1D nanostructure, hollow vesicles also can exhibit supramolecular chirality. The dumbbell-shaped molecule consisting of oligo(*p*-
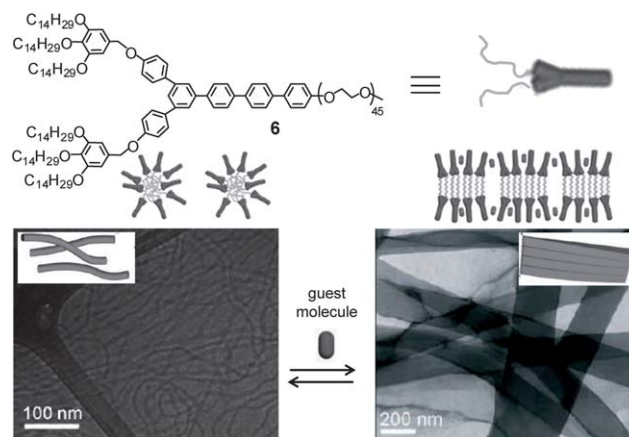
Fig. 4 Molecular structure of amphiphile **6**, TEM images and schematic representation of the transformation of single nanofibers to flat ribbons, driven by addition of aromatic guest molecules. Reproduced with permission from ref. 42. Copyright 2008 Wiley-VCH.

phenylene vinylene) (OPV) as a hydrophobic rod and two hydrophilic dendrons at both ends self-assembles into hollow capsules, which is concomitant with a clear Cotton effect.[41] Despite that the vesicular aggregates are still stable on heating at 90 °C, the CD signal gradually disappears. This finding indicates that supramolecular chirality is expressed in the spherical aggregate. The authors proposed that the vesicles are presumably composed of domains of helical OPV aggregates at low temperature, as observed for thiophene vesicles. With increasing temperature, disorder is introduced at the molecular level while strong hydrophobic forces hamper vesicle disruption at the microscopic level, leading to the disappearance of the chiral signal within the vesicles.

The introduction of a branched alkyl chain and a linear PEO chain into each end of a wedge-shaped rigid aromatic segment (**6**) gives rise to flexible fibers with uniform diameter that subsequently entangle with each other to form hydrogel.[42] When a sample was cast from 0.01 wt% aqueous solution and then negatively stained with uranyl acetate, the TEM image showed cylindrical fibers of 19 nm in diameter. Cryo-TEM image revealed that the dark cylindrical fibers have a uniform diameter of 10 nm (Fig. 4), suggesting that the hydrophobic core consists of twice the length of the hydrophobic segments including the rod unit and the alkyl chain. Combining the TEM results together with the molecular model of **6**, it can be concluded that the aromatic units in the cylindrical cores stack in a radial way, which provides for the space-filling requirements for the long PEO chains. Interestingly, addition of aromatic guest molecules induces the flexible nanofibers to transform into flat ribbon structures (Fig. 4), resulting in gel–sol transition. The reason is that the addition of guest molecules into the hydrophobic core enforces the radial arrangement of the aromatic units to adopt a parallel packing to load the guest efficiently, leading to elementary fibers with hydrophobic side faces. Subsequently, the elementary fibers stack laterally into a rigid ribbon structure to reduce the exposure of the hydrophobic side faces to a water environment. It is not easy for the
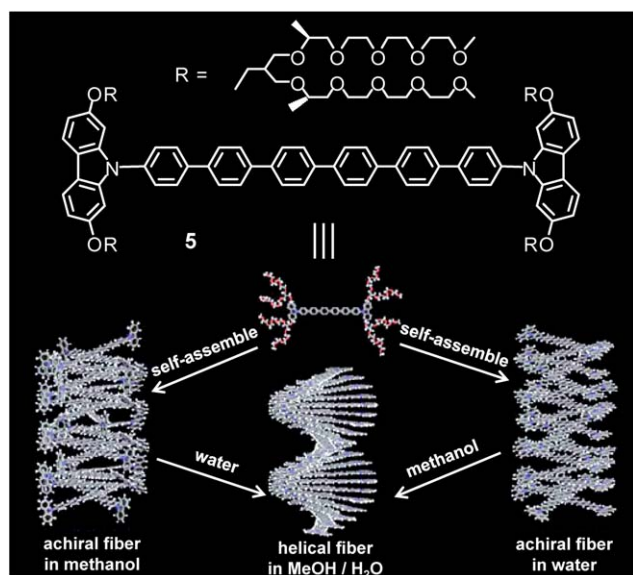

Fig. 3 Molecular structure of dumbbell-shaped amphiphile **5**, and schematic representation of structural interconversion between helical and straight fibers. Reproduced with permission from ref. 40. Copyright 2011 Royal Society of Chemistry.

rigid ribbons are to entangle with each other, driving the gel-to-sol transition.

3 Aqueous assembly from laterally grafted rod–coil amphiphiles

In addition to the volume fraction, the molecular shape also has a pivotal influence on the self-assembly of rod–coil block molecules. In the bulky state, the laterally grafted rod-like liquid crystals exhibit different orientational order and new self-assembly morphologies.[43,44] The vast amount of knowledge gained from the study of the bulk state has been applied to the research of aromatic rod–coil in the aqueous state. Lee and co-workers designed and synthesized a laterally grafted rod amphiphile (7) consisting of a hepta(p-phenylene) rod in which hydrophilic oligoether dendrons and hydrophobic branched heptyl chains were grafted opposite to each other at the midpoint of the rod-like scaffold (Fig. 5). The authors reported the formation of a sheet-like structure.[45] Cryo-TEM and atomic force microscopy (AFM) revealed that the thickness of 2D sheets is 5.4 nm, indicating that the amphiphilic rods are packed in a bilayer arrangement in the 0.01 wt% aqueous solution of 7, in which the arrangements of rod units are parallel to the sheet planes. As an extension of this work, they find that the sheets of 7 break-up into toroidal micelles upon addition of rod amphiphile 8 containing only a hydrophilic chain (Fig. 5), indicating that the 2D sheet transforms into discrete nanostructures with a hollow interior triggered by coassembly.[46] The structural transformation from planar sheets to discrete toroids upon addition of 8 can be explained by the increasing volume fraction of hydrophilic segments through hydrophobic and π–π interactions between 7 and 8. To relieve the steric crowding at the flat rod–coil surfaces, the 2D sheets dissociate into discrete aggregates with more highly curved interfaces. The observed dimension of the internal cavity together with the molecular length indicate that the toroids are composed of a hydrophobic interior with a diameter of 2 nm and a hydrophilic exterior with a diameter of 10 nm. Notably, the formation of water-soluble toroids with hydrophobic cavity would encapsulate nano-sized guest molecules in aqueous solution. As shown in Fig. 5, the addition of hydrophobic C_{60} guests into a coassembly solution of 7 and 8 drives the discrete toroids to stack on top of one another to form a 1D tubular structure. The TEM image of the mixed solution containing 30 mol% C_{60} shows that individual toroid rings with a height of 3.3 nm stack along the cylinder axis to form a tubular container with a diameter of 10 nm. This finding demonstrates that the nano-sized fullerenes are encapsulated within the internal cavity. Encapsulation of fullerene would force the toroidal rings to be more hydrophobic at the top and bottom. To reduce the contact of the hydrophobic parts of the rings to a water environment, the rings self-associate in a 1D manner to form elongated tubules. As a result, the fullerene array can be attained within the 1D spatial confinement of the hollow tubule. This work represents a good example of directional assembly of discrete nanostructures controlled by an applied stimulus.
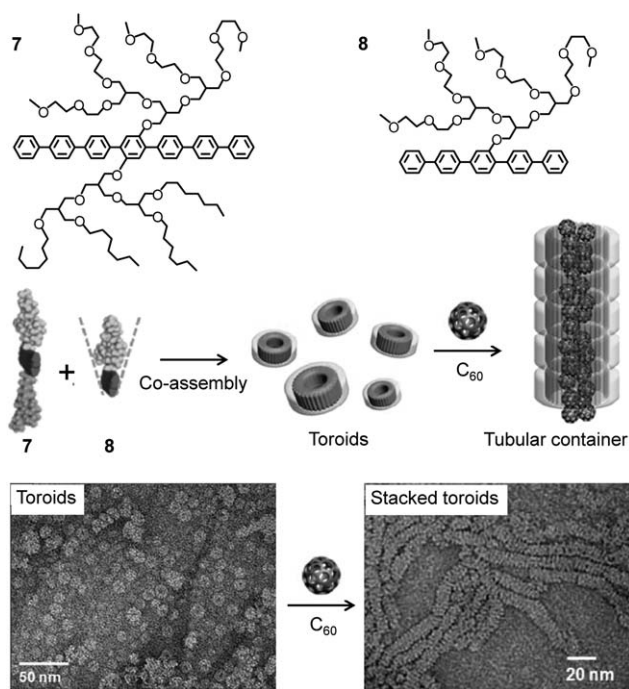

Fig. 5 Molecular structures of amphiphiles 7 and 8, TEM images and schematic illustration of the transformation from toroids to 1D tubules upon addition of C_{60} guest molecules. Reproduced with permission from ref. 46. Copyright 2009 American Chemical Society.

The above results show clearly that the self-assembled architectures are dominated by uni-directional guiding of the aromatic rods. Elaborate construction of supramolecular nanostructures requires a rational design of the topology of the elongated aromatic rods. With this idea in mind, Lee and co-workers synthesized a laterally grafted bent-rod amphiphile 9 consisting of a meta-linked aromatic segment and an oligoether dendron side-group (Fig. 6).[47] They present the formation of hexameric macrocycles, which stack on top of each other to form an elongated tubular structure. TEM image of aqueous solution of 9 (0.005 wt%) shows the formation of 1D cylindrical aggregates with a uniform diameter of 6.5 nm and lengths of several micrometers. The top-view image reveals that the cylinders have a hollow interior with a diameter of 3 nm (Fig. 6). The CD spectra of the aqueous solution of 9 display a significant Cotton effect in the spectral region of the aromatic units, thus indicating the formation of one handed helical tubules. Considering the TEM results and molecular dynamics simulations, it can be proposed that the bent-shaped aromatic units of 9 are arranged into a single slice and the terminal nitrile end groups are located at the bay position of the adjacent molecule to form a hexameric macrocycle. The macrocycles stack together with mutual rotations at an angle of 16.5° in the same direction to give rise to chiral tubules with hydrophilic oligoether dendritic chains exposed to the water environment. These helical tubules are segmented into discrete toroids with a diameter of approximately 8 nm upon addition of guest molecule (Fig. 6). More importantly, helical order is maintained in these small nanostructures. The

preservation of the shape-persistent hexameric macrocycles during this transition is responsible for the retention of supramolecular chirality.
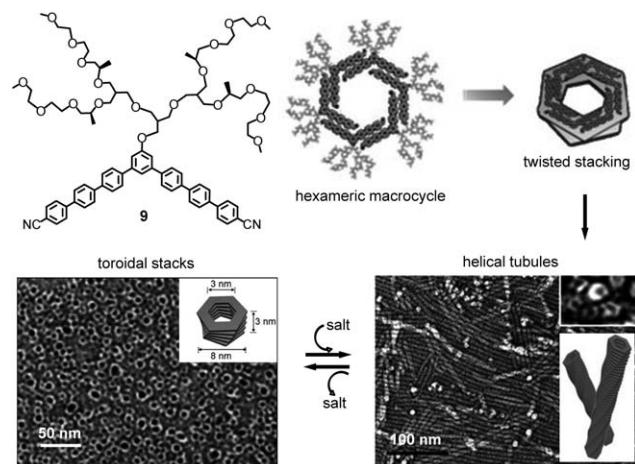

Fig. 6 Molecular structure of amphiphile **9**, TEM images and schematic representation of the structural transformation from helical tubules to discrete toroids upon addition of salts. Reproduced with permission from ref. 47. Copyright 2010 Wiley-VCH.

In another example, the researchers synthesized self-assembling molecule **10** consisting of a long bent-shaped rod segment containing *m*-pyridine units at both ends and a hydrophilic oligoether dendron with an *S* configuration grafted at the apex (Fig. 7).[48] The introduction of pyridine units at the end of the bent-shaped aromatic segment results in a supramolecular switching between flat sheet and helical tubules triggered by metal ions. TEM image of **10** shows flat sheets with regular stripes having a periodicity of 2 nm (Fig. 7). This result suggests that the aromatic units of **10** adopt a zigzag conformation with a parallel orientation to the sheet plane. Considering the inter-apex distance of 3.7 nm within the zigzag conformation as obtained from molecular modelling, it can be concluded that the adjacent aromatic segments are slipped relative to each other with an angle of 57.4° to relieve the steric crowding between the dendritic chains. The CD spectra of the aqueous solution of **10** show a silent Cotton effect even though in the presence of chiral side groups, which is predictable for symmetric 2D objects. However, addition of silver salt to the solution of **10** induced significant CD signals, suggesting that the 2D sheets transform into chiral superstructures. Interestingly, the CD signals immediately disappeared upon the addition of tetra-*n*-butylammonium fluoride, indicating that this transformation is reversible over many cycles. The structural transformation was also confirmed by TEM and AFM. As shown in Fig. 7, helical objects with a diameter of 7 nm and a left-handed sense with a pitch of 3 nm are observed upon adding Ag(ɪ) ions. Combining the ^{1}H NMR, DLS, vapour pressure osmometry (VPO), and concentration-dependent TEM measurements, it was proposed that the coordination interaction between Ag(ɪ) ion and pyridine groups leads to the

formation of dimeric macrocycles in diluted aqueous solution. With increasing concentration, the dimeric macrocycles stack on top of each other to form helical tubules. Thus, the most notable feature of molecule **10** is its ability to respond to metal ions by a structural change from nonchiral 2D sheet to chiral 1D tubule.
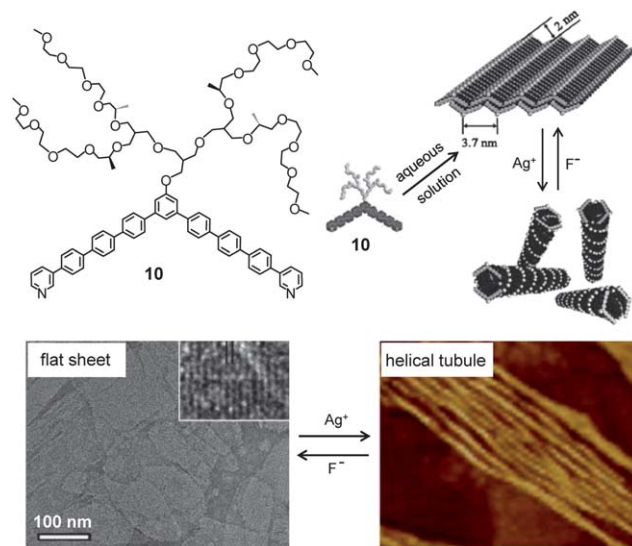

Fig. 7 Molecular structure of amphiphile **10**, TEM and AFM images, and schematic illustration of the transformation from 2D flat sheets to helical tubules with addition of salts. Reproduced with permission from ref. 48. Copyright 2013 American Chemical Society.

Recently, the laterally grafted molecular design has been extended to flat disc-shaped aromatic segments. This would introduce face-to-face interactions into the self-assembly process through side-by-side arrangements of the molecular building block.[20,49] Lee and co-workers have elegantly designed laterally grafted block molecule **11** consisting of a flat aromatic bicycle with a hydrophilic dendron on the center of the basal planes (Fig. 8).[50] They report the spontaneous formation of 2D porous sheets in aqueous solution. The TEM images show the formation of flexible sheets in a bulk solution of **11**. The high magnification TEM image shows that the rugged surface consists of uniform micelles together with in-plane nanopores, implying that the flat sheets stem from a lateral association of discrete micelles (Fig. 8). The polymerization of diacetylene groups by UV irradiation to the aqueous solution of **11** yielded only a dimeric product. VPO measurements also show the presence of a dimeric aggregate. The collective results suggest that the 2D sheets consist of dimeric micelles, in which the two aromatic segments are facing each other. The porous sheet structures are attributed to the weak lateral association of the dimeric micelles arising from a slipped π–π stacking, leading to in-plane defects. Interestingly, the porous sheets transform into closed sheets upon the addition of a flat coronene molecule. The reversible switch of the pores has important potential for pumping molecules.
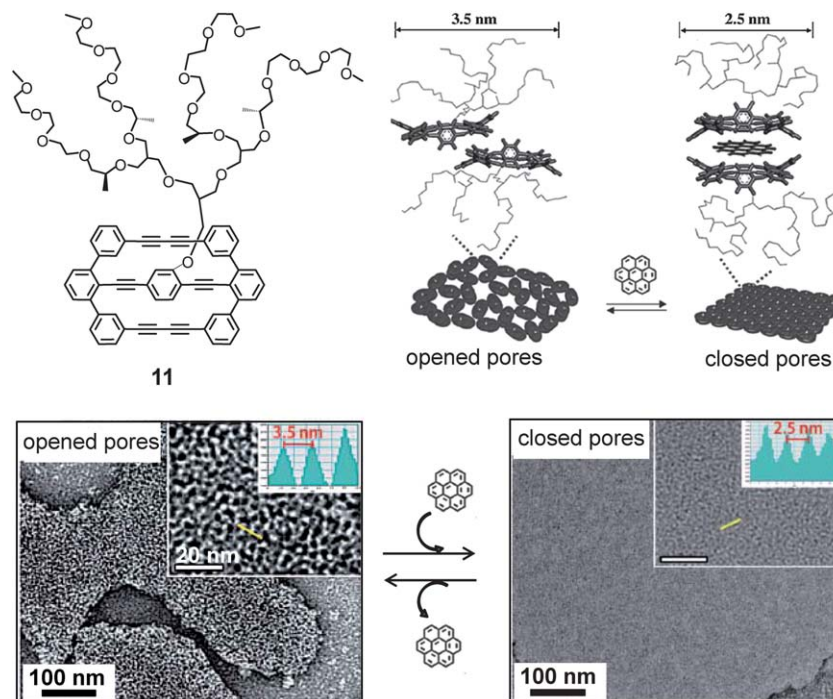
Fig. 8 Molecular structure of amphiphile **11**, TEM images and schematic illustration of the transformation from open-porous sheets to closed-sheets in response to the addition of aromatic guest molecules. Reproduced with permission from ref. 50. Copyright 2013 Wiley-VCH.

4 Dynamic nanostructures triggered by temperature

The aqueous nanostructures obtained from aromatic block molecules allow the construction of dynamic self-assemblies triggered by temperature because of the LCST behavior of the oligoether chains.[34] At room temperature, the ethylene oxide chains are fully hydrated and thus hydrophilic. Above the LCST, however, the ethylene oxide chains would be dehydrated due to the breaking of the hydrogen bonding between ether oxygens and water molecules. Consequently, the ethylene oxide chains would collapse into molecular globules, which enhances the surface energies and causes the aqueous nanostructures to become switchable. This concept has been extended to construct porous capsules with reversibly gated lateral pores from dumbbell-shaped rod amphiphiles, which offer novel opportunities for controlling delivery vehicles.[51] Recently, Lee and co-workers have synthesized a rod–coil amphiphile **12** consisting of a penta-*p*-phenylene rod and a laterally grafted dendritic oligoether chain through an imidazole linkage (Fig. 9).[52] The TEM image obtained from a 0.01 wt% aqueous solution of **12** shows the formation of nanofibres with a uniform diameter of ∼9 nm and lengths of several micrometres. Combining the X-ray diffraction experiments and Corey–Pauling–Koltun (CPK) models, it can be concluded that the nanofibres consist of aromatic cores surrounded by hydrophilic dendritic chains. Within the 1D hydrophobic interior, the rod segments are directed parallel to the fibre axis and aligned with a nematic-like slipped arrangement (Fig. 9). Remarkably, the transparent nanofibre solution of **12** at a concentration above 0.8 wt% transforms into a turbid gel state upon heating. Cooling down

the temperature leads to a reversible gel-to-sol transition. The optical polarized micrograph of the gels shows strong birefringence with a thread-like texture, indicative of the formation of nematic arrangements. The TEM image of the gel reveals parallel alignments of the nanofibres at higher temperatures (Fig. 9). The collective findings demonstrate that the two states have different nanofibre alignments. This sol–gel transition can be explained by the entropically driven dehydration of the oligoether segments. The dehydration induced by heating makes the surface of the nanofibres more hydrophobic, thus driving the adjacent nanofibers to interconnect with each other through enhanced hydrophobic interactions. Dynamic viscoelasticity measurements show that the hydrogels have a large stiffness, with 120 Pa in storage modules, which originates from the formation of supramolecular nanofibres with a high persistent length imparted by the nematic substructure of the rod segments aligned along the fibre axis. Notably, these thermoresponsive hydrogels have the ability to encapsulate and release cells that provides the potential for *ex vivo* cellular scaffolds.

To explore further the dynamic features, the researchers synthesized amphiphilic molecule **13** based on an elliptical macrocycle that can endow aggregates with a responsive character through a conformation change triggered by temperature (Fig. 10).[53] The TEM image shows that molecule **13** self-assembles into cylindrical fibers in aqueous solution. Subsequently, the fibers fold into highly curved helical coils with a diameter of ∼30 nm and a helical pitch of ∼10 nm (Fig. 10). The CD spectra of the helical coil display a strong Cotton effect over the absorption ranges, suggesting that the assembly has a preferred handedness. Notably, the obtained helices transform into straight rods upon heating. As shown in Fig. 10, the cryo-TEM
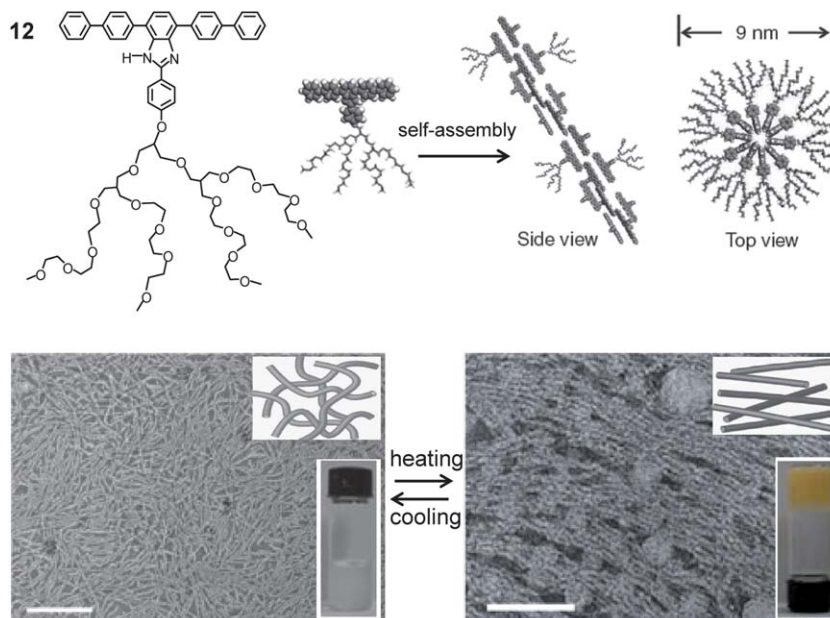
Fig. 9 Molecular structure of amphiphile **12**, TEM images and schematic illustration of the transformation of the sol–gel interconversion triggered by temperature. Reproduced with permission from ref. 52. Copyright 2011 Macmillan Publishers Limited.

image reveals the presence of straight cylinders with a uniform diameter of 3 nm upon heating the aqueous solution of **13** to 50 °C. This switching behavior between helical coils and straight cylinders arises from the conformational change of the elliptical macrocycle caused by LCST of the hydrophilic chains. As confirmed by molecular dynamic simulations (Fig. 10), the elliptical macrocycle has a boat conformation at room temperature. The non-planar macrocycles stack with a slightly slipped and staggered arrangement with respect to their neighbors to form highly curved helical aggregates. Above LCST, the enhanced hydrophobic interactions enforce the aromatic cycle to adopt a compromising conformation with flat shape that stack together to form 1D straight fibers.
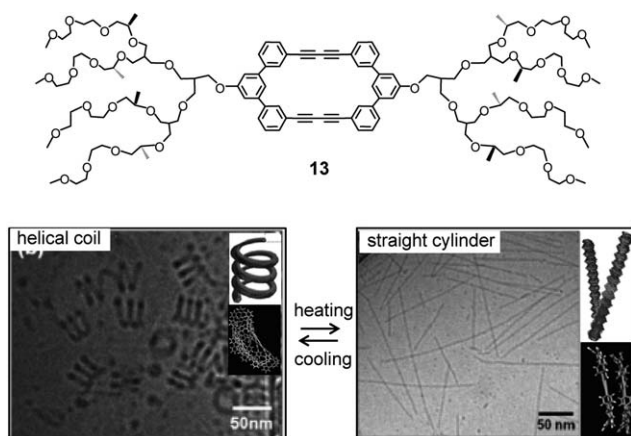

Fig. 10 Molecular structure of amphiphile **13**, TEM images, schematic illustration and molecular modelling of reversible transformation of helical coils and straight cylinders. Reproduced with permission from ref. 53. Copyright 2009 American Chemical Society.

Hollow tubular structures, such as bioactive channels and cytoplasmic microtubules are ubiquitous in nature.[54] Inspired by biological systems, analogous structures have been synthesized using supramolecular chemistry.[55,56] Nonetheless, artificial nanotubules with stimuli-responsive action remain a significant challenge because such structures are either too rigid to allow major structural changes or too flimsy to remain intact during environmental changes. Recently, Lee and his colleagues created a pulsating nanotubule from a sophisticated molecular design.[57] The researchers start with an aromatic block molecule **14** consisting of a bent-shaped rod segment with a pyridine unit at the valley position and a hydrophilic dendron grafted at its apex (Fig. 11A). TEM and AFM results show that the bent-shaped rod–coil molecules can self-assemble into a hexameric ring in aqueous solution and then spontaneously stack together into elongated helical tubules with an external diameter of 11 nm and internal diameter of 4 nm (Fig. 11B). Detailed investigations demonstrate that the hexameric ring consists of rod segments with slipped packing because the pyridine centre nucleates water molecules through hydrogen bonding in the interior of the ring. On heating to 60 °C, however, the tubular structure undergoes an obvious contraction. The density profile taken perpendicular to the long axis of the tubule shows that the external and internal diameters are 7 and 3 nm, respectively, indicating a 47% shrinkage with respect to that at room temperature. This tubular shrinkage and swelling are fully reversible on subsequent cooling and heating cycles, creating smart tubules with a breathing motion (Fig. 11C). Two factors cause this system expansion–contraction motion. First, the looser packing of aromatic units in the hexameric ring allows the changes in diameter. Second, the water cluster can be broken and the water molecules are extruded out of the

interior of the tubule upon heating. The dehydration process allows the sliding of the aromatic segments from the slipped arrangement into the fully overlapped motif to maximize the hydrophobic interactions. The breathing motion of the tubules has been utilized to pump hydrophobic guest molecules out of their interior by controlling the temperature. More interestingly, this dynamic feature of the tubules is accompanied by chirality inversion. The CD spectrum of **14** shows a negative Cotton effect at 369 nm. Upon heating, however, an opposite Cotton effect is observed at 369 nm (Fig. 11D), which is consistent with the CD signal of the molecule enantiomer. AFM measurements demonstrate that the tubules comprising **14** have a right-handed helical structure that is a mirror image of the tubules comprising the *R*-enantiomer. These collective findings suggest that the helical sense of **14** switches to opposite handedness triggered by temperature. This thermo-responsive helical system represents a significant contrast to other dynamic helical structures, which show a simple extension–contraction motion or fold into a random coil conformation with loss of supramolecular chirality.[58,59]

When one side of the one-dimensional β-strand consists of hydrophobic residues, the hydrophobic interactions between the side faces drive two β-strands to associate into stable bilayer structures. Based on these facts, the β-sheet can be considered as a kind of rod segment for the design of novel rod–coil block molecules. Examples of these peptide block molecules have been provided by grafting hydrophilic chains, such as ethylene oxide chain or cell penetrating peptide chain (CPP), on a β-sheet segment.[62–64] These works showed the perspective that block peptides can be developed as new building blocks. Recently, Lee and co-workers reported a kind of T-shaped block peptide **15** consisting of a peptide backbone and a hydrophilic dendron at the central part (Fig. 12).[65] The peptide backbone has a repeating structure of tryptophan, lysine, tryptophan and glutamic acid groups, which has been confirmed to promote the β-sheet formation. The TEM image reveals that peptide **15** forms discrete nanorings. The cross-section of the nanorings is about 4 nm (Fig. 12), corresponding to the width of a fully extended peptide. These results suggest that the nanorings are composed of a single layer of β-strand peptides with an end-to-end connection. It was concluded from a comparative experiment that the highly interfacial curvature originates from the bulky effects of the hydrophilic dendron. The obtained nanoring structures are similar to natural β-barrel proteins. Inspired by this finding, peptide **16** with hydrophobic dendrons (Fig. 12) was prepared for exploring ionic channels in lipid bilayer membranes.
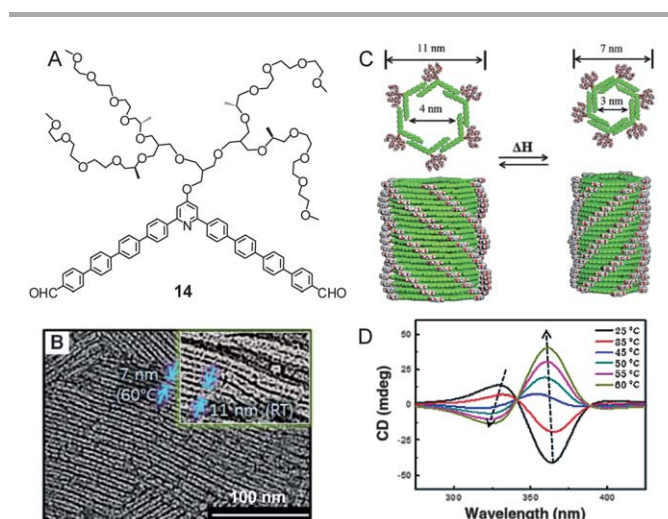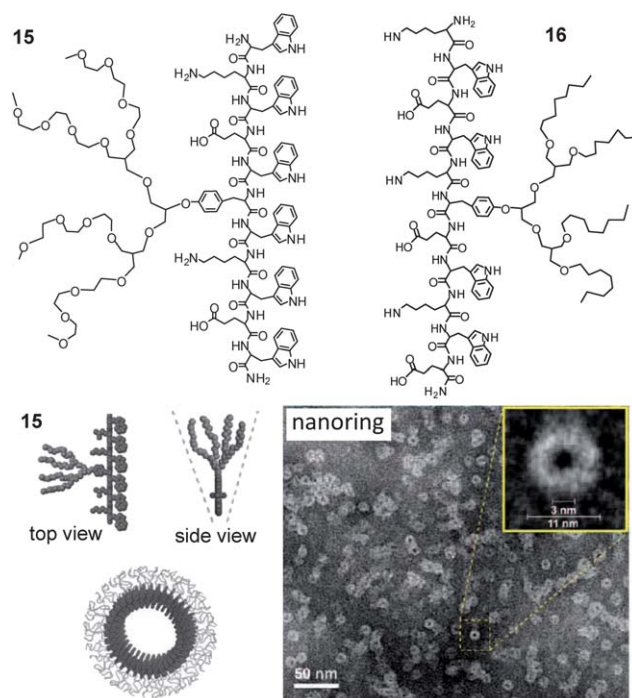

Fig. 11 (A) Molecular structure of amphiphile **14**; (B) TEM images for the tubules with an expansion–contraction motion in response to temperature change; (C) schematic illustration of reversible switching of the tubules between expanded and contracted states with chirality inversion; (D) temperature-dependent CD spectra of **14** in 0.01 wt% aqueous solution. Reproduced with permission from ref. 57. Copyright 2012 American Association for the Advancement of Science.

5 Aqueous assembly from bioactive rod–coils

Artificially designed β-sheet peptides have gained continuous attention as biomaterials because of the fact that they are composed of biocompatible amino acids.[60] Most artificial β-sheet peptides usually consist of alternating hydrophobic and hydrophilic (or polar) amino acids.[61] This type of arrangement promotes the formation of a proper hydrogen-bonding arrangement between amide hydrogen and carbonyl oxygen, resulting in an extended conformation in backbone.

Fig. 12 Molecular structures of block peptides **15** and **16**, TEM images and schematic illustration of the formation of nanorings. Reproduced with permission from ref. 65. Copyright 2011 Wiley-VCH.

In another example, a photo-responsive block peptide was designed to modulate the gel–sol transformation. Peptide amphiphile **17** consists of hydrophobic phenylalanine-4′-azobenzene units, tri(ethylene glycol) modified tyrosine as hydrophilic units, and two lysine groups placed at both ends (Fig. 13a).[66] The alternating placement of the hydrophobic and hydrophilic residues in peptide **17** results in the formation of a typical β-sheet conformation as confirmed by CD and FT-IR spectra. A TEM image revealed that the β-sheet block molecules self-assemble into long nanofibers with a uniform diameter in diluted aqueous solution. With increasing concentration, the nanofibers entangle with each other to form a stable hydrogel with 3D networks (Fig. 13b). Considering the X-ray diffraction and molecular models, it is proposed that the nanofibers consist of a bilayer structure with intercalated azobenzene units. Notably, the obtained gels have the ability to respond to UV irradiation, leading to the formation of a fluid solution. This conformational change caused by photoisomerization of azobenzene side groups enforces the long nanofibers to disassociate into discrete spherical aggregates (Fig. 13c), driving the gel-to-sol transformation. It is concluded in this system that the electrostatic repulsions between the protonated lysine units play a crucial role in promoting the disassociation of nanofibers. The nanofibers of the peptide gel are able to encapsulate guest molecule such as Rhodamine B, showing the possibility of use in drug delivery applications.

exploring multivalent interactions.[68] In recent years, self-assembled nanostructures of rod–coil amphiphiles have begun to emerge as multivalent scaffolds for carbohydrate coatings.[69,70] The rod–coil amphiphiles **18–20**, which consist of tetra-*p*-phenylene as rod segments and conjugated mannose units at the end of poly(ethylene oxide) chains as coil segments (Fig. 14), show significant structural changes from cylindrical micelles (**18**) to spherical micelles (**19**) and vesicles (**20**). The mannose-decorated nanostructures were shown to act as multivalent ligands in the presence of mannose-binding lectin protein, concanavalin A (Con A). TEM observations show that all the supramolecular objects are surrounded by lectin proteins. Such a specific binding event was found exclusively in mannose-decorated nanostructures, as the control experiment with non-specific galactose-decorated objects did not show any specific object-Con A association behavior. The hemagglutination inhibition assay with Con A shows that the size and shape of the supramolecular objects have a significant effect on the binding activity. The dependence of object size and shape in supramolecular multivalent interactions has also been extended to investigate the carbohydrate-bacterial cell interaction system. A triblock rod–coil molecule **21** consisting of an aromatic rod, carbohydrate (mannose) dendrons and a hydrophobic alkyl chain was utilized to corroborate the carbohydrate–bacterial cell interaction (Fig. 14).[71] Such a building block self-assembles into carbohydrate-coated cylindrical nanostructures with a
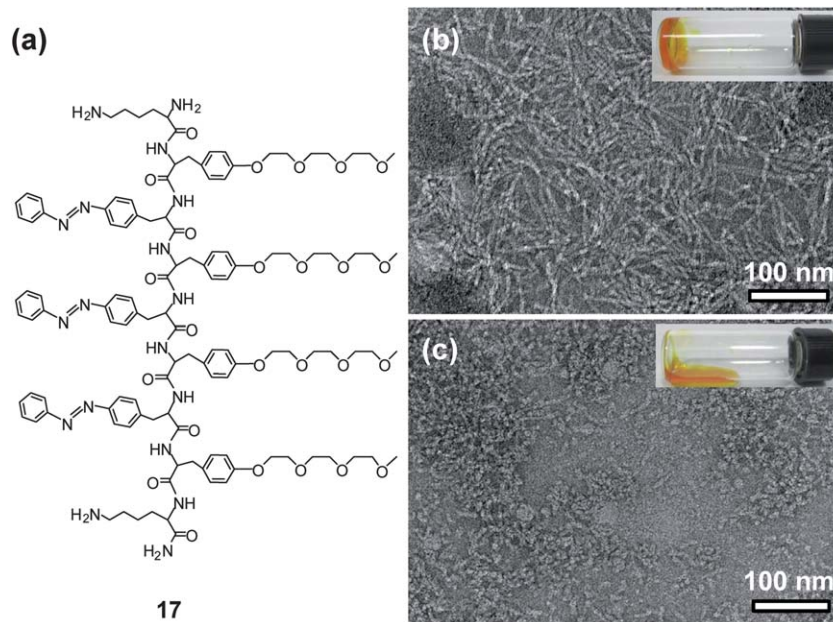

Fig. 13 (a) Molecular structure of block peptide **17**; (b) TEM image of **17** in aqueous solution (inset: optical image of **17** gel sample); (c) TEM image of **17** solution after exposing to 360 nm UV light for 20 min (inset: optical image of **17** sol sample). Reproduced with permission from ref. 66. Copyright 2012 Royal Society of Chemistry.

In addition to peptide segments, carbohydrates have been identified as another important class of bioactive groups. There are many biological events that depend on carbohydrate-mediated interactions.[67] They generally achieve their specificity by

length of ∼200 nm in aqueous solution. Remarkably, these cylindrical structures are able to transform into spherical objects upon addition of hydrophobic guest molecules. Investigation on the interactions between *Escherichia coil* (*E. coli*) cell

and the mannose-coated nanostructures show that both nano-objects could inhibit the motility of bacteria; however, the inhibiting capability is dependent on the shape and size of the nanostructures.
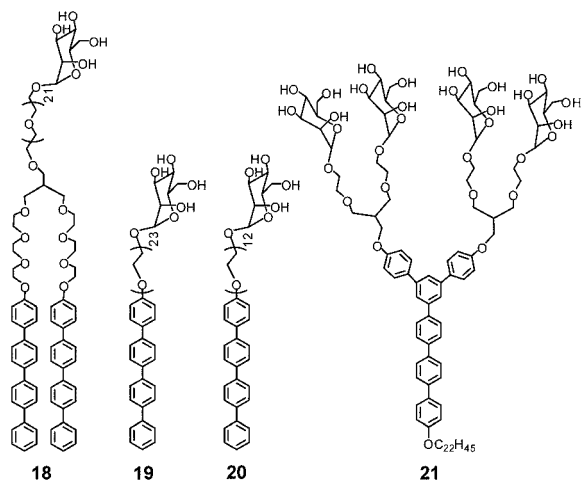
Spectrophotometric experiments show that the proliferation efficiency of bacterial cells is strongly dependent on the length of mannose-coated nanofibers.
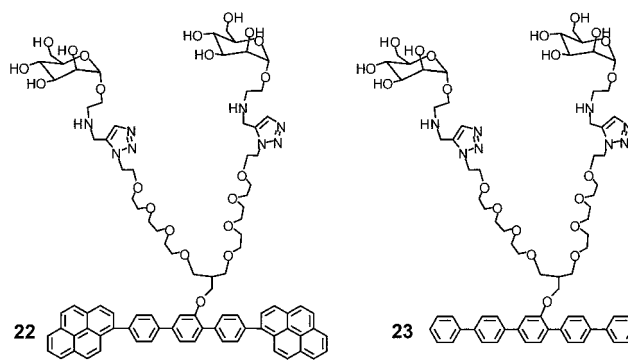

Fig. 14 Molecular structures of rod–coil amphiphiles **18–21**.

Fig. 15 Molecular structures of amphiphiles **22** and **23**.

Based on the above results, it can be anticipated that the self-assembled nanostructures have the ability to crosslink and thereby agglutinate bacterial cells if the nanoobjects are longer than bacterial cells. Substantiation of this idea has recently been described by a co-assembly strategy.[72] Carbohydrate rod amphiphiles **22** and **23** were synthesized as self-assembled building blocks (Fig. 15). Molecule **22** with highly crystalline rod self-assembles into long and rigid nanofibers with uniform width of ∼6 nm and length of >2 μm. In contrast, **23** forms very short fibers with an average length of 70 nm. When mixing the two block molecules together with **22** : **23** mole ratios of 85 : 15, 50 : 50, and 0 : 100, the length of nanofibers systematically decreases from 1 μm to 300 nm to 70 nm. The replacement of pyrene units with phenyl units through coassembly reduces the π–π interactions between aromatic segments, thereby causing the disruption of the packing of the aromatic segments. To investigate the multivalent interactions between the nanofibers and bacterial cells, an *E. coli* strain expressing the mannose-binding adhesion protein FimH in its type-1 pili (ORN 178-GFP) was chosen. When the *E. coli* are incubated with pure **22**, the coassembled samples, and pure **23**, respectively, clusters of fluorescent bacteria with different sizes are observed. As shown in Fig. 16, the size of the fluorescent cluster decreases with a decrease of the fiber length. For sample **23**, no clear bacterial agglutination was observed. Agglutination index (AI) assays also show that the AI values gradually increase with increasing **23** content. These findings indicate that long nanofibers have the ability to aggregate *E. coli* cells dispersed in media, forming large bacterial clusters. However, short fibers are not able to aggregate *E. coli*. In addition to the agglutination function, the coassembled nanofibers are able to regulate the bacteria proliferation.

6 Conclusions and outlook

The self-assembly behavior of rod–coil block amphiphiles has provided powerful tools to create various nanostructures in aqueous solution, including micelles, vesicles, nanorings, porous capsules, helical fibers and tubules, and 2D flat sheets. Systematic studies show that the unique morphologies are dependent on the relative volume fraction of hydrophobic and hydrophilic blocks, the molecular structure and the topology of aromatic segments. The most salient features of the rod–coil amphiphiles originates from the anisotropic orientation of the rigid rod segments, the LCST behavior of oligoether oxide flexible chains, and the strong phase segregation of both segments. Hence, the structural and property changes of the nanostructures can be triggered by small environmental variations toward responsive supramolecular materials. Although the reported results provide quite significant insight to the understanding of the driving forces behind molecular self-assembly, ongoing research efforts are still necessary in the rational design of rod–coil building blocks to find the exact structure–property relationships. In particular, the dynamic properties of the self-assembled structures to various types of conceivable external stimuli, besides temperature, should be consistently explored.

The aqueous nanostructures with bioactive groups (peptides and carbohydrates) are beginning to show significant potential in the exploration of biosimulation, ion transport, guest release, and the regulation of agglutination and proliferation of bacterial cells. These properties can offer novel opportunities in the development of self-assembled nanostructures as useful biomaterials. The size and morphology of the aqueous nanostructure have an important influence on their biological functions. Therefore, the physical properties of the bioactive nanostructures should be able to be controlled in an intuitive manner. In this aspect, the bioactive nanostructures of the rod–coil amphiphiles together with their responsive properties might allow the exploration of undefined bioprocesses and expand the repertoire of biomaterials applications.
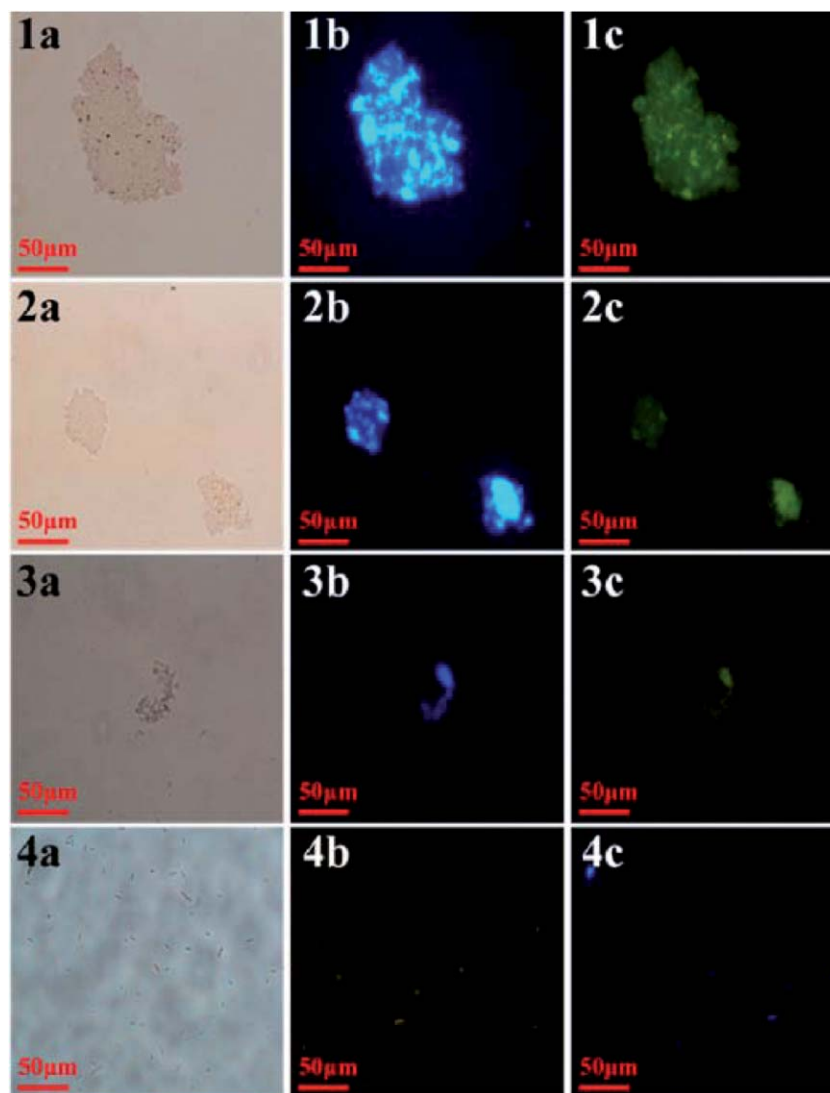
Fig. 16 Microscopy images from fluorescence colocalization studies of *E. coli* (yellow) with nanofibers (blue): (a) bright-field, (b) fluorescence (excitation filter at λ_{ex} = 450–490 nm), and (c) fluorescence (excitation filter at λ_{ex} = 340–380 nm) images for incubation with (1) **22**, (2) **22** : **23** = 85 : 15, (3) **22** : **23** = 50 : 50, and (4) **23**. Reproduced with permission from ref. 72. Copyright 2012 American Chemical Society.

Acknowledgements

Notes and references

1 T. Aida, E. W. Meijer and S. I. Stupp, *Science*, 2012, **335**, 813–817.

2 X. Z. Yan, F. Wang, B. Zheng and F. H. Huang, *Chem. Soc. Rev.*, 2012, **41**, 6042–6065.

3 Y. Cui, S. N. Kim, R. R. Naik and M. C. Mcalpine, *Acc. Chem. Res.*, 2012, **45**, 696–704.

4 J. T. Davis and G. P. Spada, *Chem. Soc. Rev.*, 2007, **36**, 296–313.

5 I. C. Reynhout, J. J. L. M. Cornelissen and R. J. M. Nolte, *Acc. Chem. Res.*, 2009, **42**, 681–692.

6 C. Wang, Z. Q. Wang and X. Zhang, *Acc. Chem. Res.*, 2012, **45**, 608–618.

7 D.-J. Hong, E. Lee, J.-K. Lee, W.-C. Zin, M. Han, E. Sim and M. Lee, *J. Am. Chem. Soc.*, 2008, **130**, 14448–14449.

8 Y. Liu, C. Yu, H. Jin, B. Jiang, X. Zhu, Y. F. Zhou, Z. Y. Lu and D. Y. Yan, *J. Am. Chem. Soc.*, 2013, **135**, 4765–4770.

9 R. J. Swanekamp, J. T. M. DiMaio, C. J. Bowerman and B. L. Nilsson, *J. Am. Chem. Soc.*, 2012, **134**, 5556–5559.

10 B. Li, J. Zhang, S. Wang, W. Li and L. X. Wu, *Eur. J. Inorg. Chem.*, 2013, 1869–1875.

11 Y. Tao, H. Zohar, B. D. Olsen and R. A. Segalman, *Nano Lett.*, 2007, **7**, 2742–2746.

12 M. Lee, B.-K. Cho and W.-C. Zin, *Chem. Rev.*, 2001, **101**, 3869–3892.

13 J.-H. Ryu, N.-K. Oh, W.-C. Zin and M. Lee, *J. Am. Chem. Soc.*, 2004, **126**, 3551–3558.

14 J.-K. Kim, M.-K. Hong, J.-H. Ahn and M. Lee, *Angew. Chem., Int. Ed.*, 2005, **44**, 328–332.

15 C. Tschierske, *Chem. Soc. Rev.*, 2007, **36**, 1930–1970.

16 F. Liu, B. Chen, U. Baumeister, X. Zeng, G. Ungar and C. Tschierske, *J. Am. Chem. Soc.*, 2007, **129**, 9578–9579.

17 Y.-B. Lim, K.-S. Moon and M. Lee, *J. Mater. Chem.*, 2008, **18**, 2909–2918.

18 H. Kim, S.-M. Jeong and J.-W. Park, *J. Am. Chem. Soc.*, 2011, **133**, 5206–5209.

19 J. B. Gilroy, D. J. Lunn, S. K. Patra, G. R. Whittell, M. A. Winnik and L. Manners, *Macromolecules*, 2012, **45**, 5806–5815.

20 S. H. Seo, J. Y. Chang and G. N. Tew, *Angew. Chem., Int. Ed.*, 2006, **45**, 7526–7530.

21 T. Shimizu, M. Masuda and H. Minamikawa, *Chem. Rev.*, 2005, **105**, 1401–1443.

22 N. L. Rosi and C. A. Mirkin, *Chem. Rev.*, 2005, **105**, 1547–1562.

23 Y.-B. Lim, K.-S. Moon and M. Lee, *Chem. Soc. Rev.*, 2009, **38**, 925–934.

24 K.-H. Han, E. Lee, J. S. Kim and B.-K. Cho, *J. Am. Chem. Soc.*, 2008, **130**, 13858–13859.

25 J.-K. Kim, E. Lee and M. Lee, *Angew. Chem., Int. Ed.*, 2006, **45**, 7195–7198.

26 L. Huang, J. Hu, L. Lang, X. Zhuang, X. Chen, Y. Wei and X. Jing, *Macromol. Rapid Commun.*, 2008, **29**, 1242–1247.

27 J.-H. Ryu, D.-J. Hong and M. Lee, *Chem. Commun.*, 2008, 1043–1054.

28 Y.-S. Yoo, J.-H. Choi, J.-H. Song, N.-K. Oh, W.-C. Zin, S. Park, T. Chang and M. Lee, *J. Am. Chem. Soc.*, 2004, **126**, 6294–6300.

29 J. Bae, J.-H. Choi, Y.-S. Yoo, N.-K. Oh, B.-S. Kim and M. Lee, *J. Am. Chem. Soc.*, 2005, **127**, 9668–9669.

30 J.-H. Ryu and M. Lee, *J. Am. Chem. Soc.*, 2005, **127**, 14170–14171.

31 W.-Y. Yang, E. Lee and M. Lee, *J. Am. Chem. Soc.*, 2006, **128**, 3484–3485.

32 J.-K. Kim, E. Lee, Z. Huang and M. Lee, *J. Am. Chem. Soc.*, 2006, **128**, 14022–14023.

33 J.-K. Kim, E. Lee, Y.-H. Jeong, J.-K. Lee, W.-C. Zin and M. Lee, *J. Am. Chem. Soc.*, 2007, **129**, 6082–6083.

34 G. D. Smith and D. Bedrov, *J. Phys. Chem. B*, 2003, **107**, 3095–3097.

35 T. Hirose, M. Irie and K. Matsuda, *Chem.–Asian J.*, 2009, **4**, 58–66.

36 I. O. Shklyarevskiy, P. Jonkheijm, P. C. M. Christianen, A. P. H. J. Schenning, E. W. Meijer, O. Henze, A. F. M. Kilbinger, W. J. Feast, A. D. Guerzo, J.-P. Desvergne and J. C. Maan, *J. Am. Chem. Soc.*, 2005, **127**, 1112–1113.

37 L. Jiang, R. C. Hughes and D. Y. Sasaki, *Chem. Commun.*, 2004, 1028–1029.

38 H. Wang, W. You, P. Jiang, L. Yu and H. H. Wang, *Chem.–Eur. J.*, 2004, **10**, 986–993.

39 J.-H. Ryu, H.-J. Kim, Z. Huang, E. Lee and M. Lee, *Angew. Chem., Int. Ed.*, 2006, **45**, 5304–5307.

40 Z. Huang, S.-K. Kang and M. Lee, *J. Mater. Chem.*, 2011, **21**, 15327–15331.

41 F. J. M. Hoeben, I. O. Shklyarevskiy, M. J. Pouderoijen, H. Engelkamp, A. P. H. J. Schenning, P. C. M. Christianen, J. C. Maan and E. W. Meijer, *Angew. Chem., Int. Ed.*, 2006, **45**, 1232–1236.

42 E. Lee, J.-K. Kim and M. Lee, *Angew. Chem., Int. Ed.*, 2008, **47**, 6375–6378.

43 I. M. Saez and J. W. Goodby, *J. Mater. Chem.*, 2005, **15**, 26–40.

44 X. H. Cheng, M. K. Das, S. Diele and C. Tschierske, *Angew. Chem., Int. Ed.*, 2002, **41**, 4031–4035.

45 E. Lee, J.-K. Kim and M. Lee, *Angew. Chem., Int. Ed.*, 2009, **48**, 3657–3660.

46 E. Lee, J.-K. Kim and M. Lee, *J. Am. Chem. Soc.*, 2009, **131**, 18242–18243.

47 H.-J. Kim, S.-K. Kang, Y.-K. Lee, C. Seok, J.-K. Lee, W.-C. Zin and M. Lee, *Angew. Chem., Int. Ed.*, 2010, **49**, 8471–8475.

48 S. Shin, S. Lim, Y. Kim, T. Kim, T.-L. Choi and M. Lee, *J. Am. Chem. Soc.*, 2013, **135**, 2156–2159.

49 J. P. Hill, W. Jin, A. Kosaka, T. Fukushima, H. Ichihara, T. Shimomura, K. Ito, T. Hashizume, N. Ishii and T. Aida, *Science*, 2004, **304**, 1481–1483.

50 Y. Kim, S. Shin, T. Kim, D. Lee, C. Seok and M. Lee, *Angew. Chem., Int. Ed.*, 2013, **52**, 6426–6429.

51 J.-K. Kim, E. Lee, Y.-B. Lim and M. Lee, *Angew. Chem., Int. Ed.*, 2008, **47**, 4662–4666.

52 Z. Huang, H. Lee, E. Lee, S.-K. Kang, J.-M. Nam and M. Lee, *Nat. Commun.*, 2011, **2**, 459–463.

53 J.-K. Kim, E. Lee, M.-C. Kim, E. Sim and M. Lee, *J. Am. Chem. Soc.*, 2009, **131**, 17768–17770.

54 F. Berthelmann, D. Mehner, S. Richter, U. Lindenstrauss, H. Lunsdorf, G. Hause and T. Bruser, *J. Biol. Chem.*, 2008, **283**, 25281–25289.

55 H. Shao, J. Seifert, N. C. Romano, M. Gao, J. J. Helmus, C. P. Jaroniec, D. A. Modarelli and J. R. Parquette, *Angew. Chem., Int. Ed.*, 2010, **49**, 7688–7691.

56 M. Schappacher and A. Deffieux, *Science*, 2008, **319**, 1512–1515.

57 Z. Huang, S.-K. Kang, M. Banno, T. Yamaguchi, D. Lee, C. Seok, E. Yashima and M. Lee, *Science*, 2012, **337**, 1521–1526.

58 E. Yashima, K. Maeda and O. Sato, *J. Am. Chem. Soc.*, 2001, **123**, 8159–8160.

59 R. B. Prince, J. G. Saven, P. G. Wolynes and J. S. Moore, *J. Am. Chem. Soc.*, 1999, **121**, 3114–3121.

60 I. Cherny and E. Gazit, *Angew. Chem., Int. Ed.*, 2008, **47**, 4062–4069.

61 K. H. Smith, E. Tejeda-Montes, M. Poch and A. Mata, *Chem. Soc. Rev.*, 2011, **40**, 4563–4577.

62 J. Hentschel, E. Krause and H. G. Börner, *J. Am. Chem. Soc.*, 2006, **128**, 7722–7723.

63 V. Castelletto and I. W. Hamley, *Biophys. Chem.*, 2009, **141**, 169–174.

64 Y.-B. Lim, E. Lee and M. Lee, *Angew. Chem., Int. Ed.*, 2007, **46**, 3475–3478.

65 I.-S. Park, Y.-R. Yoon, M. Jung, K. Kim, S. B. Park, S. Shin, Y.-B. Lim and M. Lee, *Chem.–Asian J.*, 2011, **6**, 452–458.

66 W. Li, I.-S. Park, S.-K. Kang and M. Lee, *Chem. Commun.*, 2012, **48**, 8796–8798.

67 C. R. Bertozzi and L. L. Kiessling, *Science*, 2001, **291**, 2357–2364.

68 L. L. Kiessling, J. E. Gestwicki and L. E. Strong, *Angew. Chem., Int. Ed.*, 2006, **45**, 2348–2368.

69 B.-S. Kim, W.-Y. Yang, J.-H. Ryu, Y.-S. Yoo and M. Lee, *Chem. Commun.*, 2005, 2035–2037.

70 B.-S. Kim, D.-J. Hong, J. Bae and M. Lee, *J. Am. Chem. Soc.*, 2005, **127**, 16333–16337.

71 J.-H. Ryu, E. Lee, Y.-B. Lim and M. Lee, *J. Am. Chem. Soc.*, 2007, **129**, 4808–4814.

72 D.-W. Lee, T. H. Kim, I.-S. Park, Z. Huang and M. Lee, *J. Am. Chem. Soc.*, 2012, **134**, 14722–14725.